DETERMINATION OF SATURATION PROFILES VIA LOW-FIELD NMR IMAGING

Michael Rauschhuber, George Hirasaki
Rice University

This paper was prepared for presentation at the International Symposium of the Society of Core Analysts held in Noordwijk, The Netherlands 27-30 September, 2009

ABSTRACT

One-dimensional oil-water saturation profiles can be determined with a low-field Maran Ultra spectrometer by implementing nuclear magnetic resonance (NMR) imaging techniques. Frequency encoding gradients impart spatial resolution to the measurements and allow for the creation of T_2 and D-T_2 profiles without having to perform multiple slice selective measurements. The first technique, denoted as RARE, relies solely on resolving transverse relaxation, T_2, as a function of height. The second method, D-T_2 profiling, allows for the determination of both the diffusion coefficient, D, and T_2 as a function of height. The ability to resolve D in addition to T_2 allows fluids with overlapping relaxation times to be distinguished, and therefore it is not necessary to use D_2O in order to differentiate the water signal from the oil signal. Implementation of these two methods allows for the determination of saturation profiles. Experiments were performed with a sandpack in order to demonstrate the applicability of these two techniques. The saturation profile of a sandpack was determined before and after 0.5 PV waterflood.

INTRODUCTION

Nuclear magnetic resonance (NMR) imaging techniques have seen increased application in core analysis. Many studies have been performed in order to determine saturation from cores using various methods. Most rely on the use of air/water systems [1] [2] or the replacement of water with heavy water in order to negate its contribution to T_2 distributions [2] [3]. Recent studies can be broadly divided into two categories based on the imaging technique applied: slice selective and frequency-encoding. One example of slice selective measurements is the repeated application of a slice selective CPMG measurement along the length of a sample in order to generate a profile [4]. However, the two methods presented in this study illustrate the use of frequency-encoding gradients to determine either T_2 or D-T_2 profiles.

Frequency encoding is a standard MRI technique used to detect spatial information from a desired sample. In a uniform magnetic field, protons precess at the same frequency, known as the Lamor frequency, f_L. When a magnetic gradient is applied, the intensity of the magnetic field and subsequently, the precession frequency varies with spatial position. For instance, under the application of a linear gradient field, the spatially dependent precession frequency can be represented by

$$f(x) = \frac{\gamma}{2\pi}\left(B_0 + g_x x\right) = f_L + \frac{\gamma}{2\pi} g_x x \tag{1}$$

Therefore, spatial information can be extracted from the sample's various precession frequencies. Consequently, g_x is referred to as a frequency-encoding gradient [5].

The ability to distinguish the different frequencies encoded into a sample is impacted by the homogeneity of the B_0. If the homogeneity of the magnet is very poor, then

positions near each other cannot be distinguished because of large variations in B_0. For a typical clinical MRI scanner, field homogeneities range from about 10 to 50 ppm over a range of 30 to 50 cm [6]. Our MARAN spectrometer has a homogeneity of about 75 ppm (or ~100 Hz) over a 4 cm length. However, at the selected frequency-encoding gradient strength (0.8 G cm^{-1}), the range in frequencies across a 4 cm is about 8 kHz. This is about a two order of magnitude difference between the variance in the static B_0 field and the bandwidth encoded in the sample, and therefore, should have little impact on the ability to distinguish nearby frequencies.

Rapid Acquisition with Relaxation Enhancement

The rapid acquisition with relaxation enhancement pulse sequence (RARE) is a CPMG-style imaging measurement first proposed by Henning et. al [7]. Presented in Figure (1) is a schematic of the pulse sequence created for the MARAN. Phase cycling for the radiofrequency (RF) pulses utilized a Cyclically Ordered Phase Sequence (CYCLOPS) in order to remove phase and amplitude errors stemming from quadrature offset [8]. The first gradient pulse is known as the pre-phasing pulse and all subsequent gradient pulses are referred to as readout pulses. Application of the prephasing gradient pulse causes spin isochromats, regions of constant precession frequency, to precess at different rates and thus get out of phase with the other isochromats. Then, the RF refocusing pulse flips all of the spins by 180°. The subsequent readout gradient plays a similar role as the prephasing gradient, causing the spins to refocus resulting in the formation of an echo [5].

The temporal location of the echo does not depend on the spacing of the RF pulses, but on the duration and magnitude of the gradient pulses. When the area under the readout pulse equals the area under the prephasing pulse, the echo will reach its maximum amplitude. Therefore, the remainder of the readout pulse acts as a prephasing pulse for the next echo [5]. In other words, the readout pulse should have twice the area of the prephasing pulse ($2g_1\delta_1 = g_2\delta_2$).

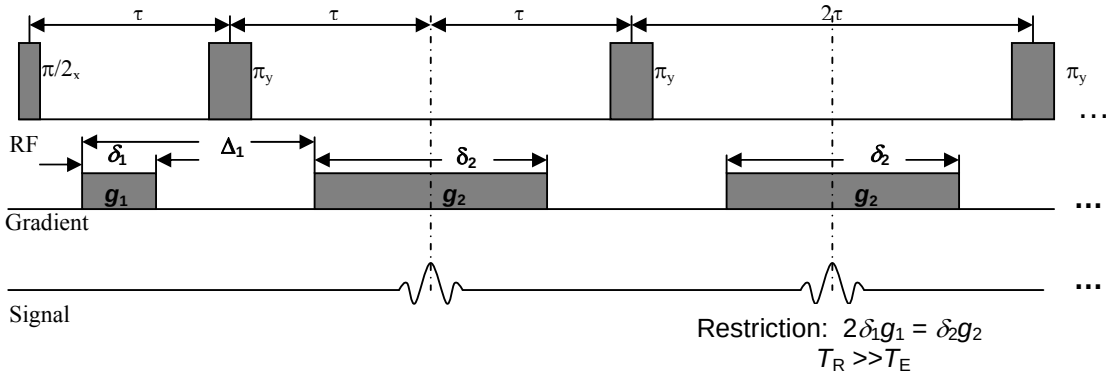

Figure 1: RARE Pulse Sequence Diagram [5].

A one dimensional profile can then be attained by performing a fast Fourier transform (FFT) reconstruction on an acquired echo [6]. Thus, the Fourier transform can be taken for each individual echo to obtain a series of one-dimensional profiles. The attenuation in the signal is also observable in the profiles, and therefore T_2 information can be determined as a function of position within the sample.

D-T_2 Profiling

Diffusion-Weighted Imaging is a MRI technique used most successfully in clinical settings to identify regions of poor blood flow in the brain [9]. However, it has the potential to be applied to porous media. Combining diffusion-weighted imaging with a sequence like RARE leads to an imaging analogue of diffusion editing. Diffusion editing has proven extremely useful in identifying saturating fluids in porous media when their T_2 distributions are overlapping [10] [11] [12].

For this work, a stimulated echo sequence was used in order to generate 1-D profiles. Use of stimulated echo allows for the use of longer diffusion times without as much loss of T_2 information in comparison to the direct echo. However, a major drawback is that the stimulated echo will have half the amplitude of its direct echo counter-part. In this work, a bipolar structure gradient structure [13] was used for both the diffusion pulses. Figure 3 shows the results from an experiment comparing the collected stimulated echo after applying the unipolar and bipolar pulses in a simple diffusion sequence. Not only did the echo generated from the pulse sequence utilizing unipolar diffusion gradients demonstrate poor shape, but the shape further deteriorated after repetition. However, the pulse sequence implementing bipolar gradients produced broad echoes that were reproducible. Therefore, the diffusion coefficients were measured in this study via bipolar gradients.

In addition to the bipolar diffusion pulses, other notable features of the pulse sequence include the separation of the diffusion and imaging sections [14] and the inclusion of a $(\pi/2)_y$ pulse during the formation of the peak of the first echo [15]. The aim of including these features is to reduce phase errors present in the collected echoes. Stimulated echoes generated by imperfect refocusing pulses can form with different phase than the primary echo due to the increased dephasing caused by the diffusion gradients [5] [15].

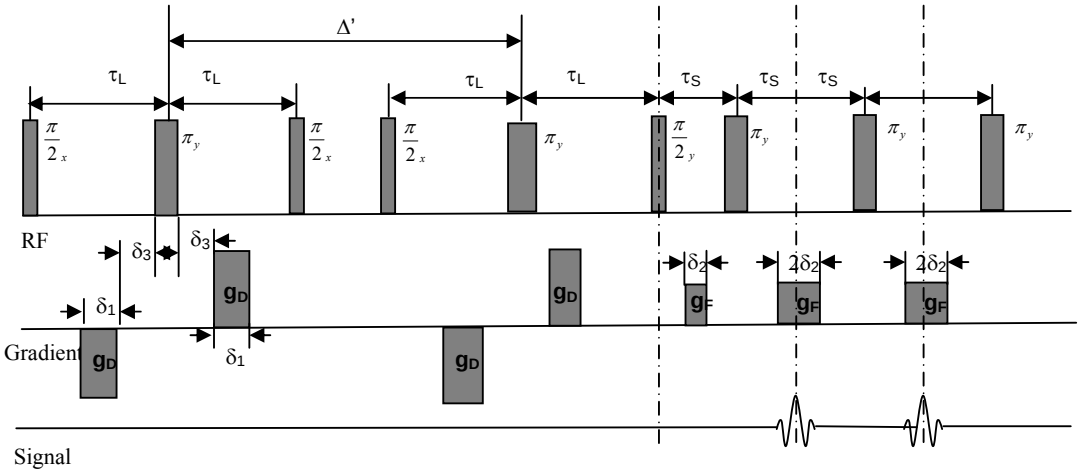

Figure 2: ***D*-T_2 profiling pulse sequence**

This can result in phase instability, which manifests itself as movement of the echo within the acquisition window and large fluctuations of the phase angle in the analysis of the FFT quadrature data. By applying a $(\pi/2)_y$ pulse, the out of phase component of magnetization will be tipped onto the longitudinal axis leaving behind the in-phase signal in the transverse plane.

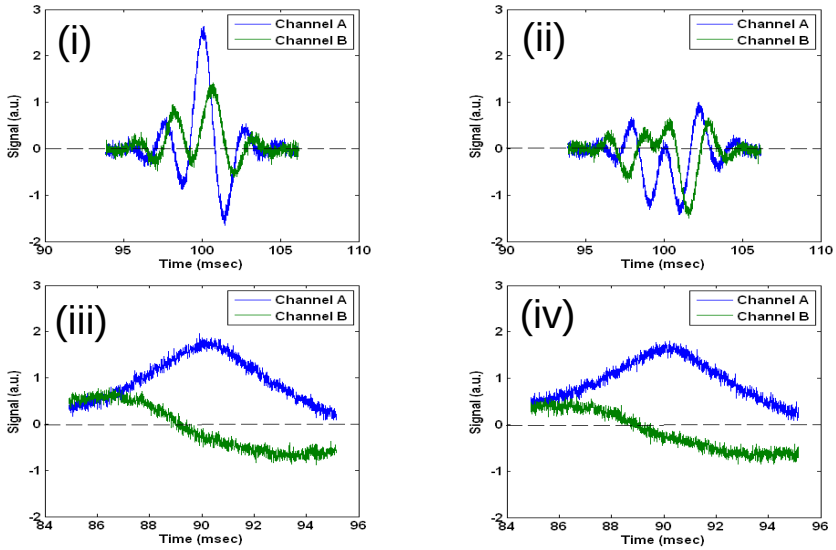

Figure 3: Effect of Unipolar vs. Bipolar Gradient Pulses in a Stimulated Echo Diffusion Sequence. Δ = 60 msec, δ = 3 msec, g = 20 G cm^{-1}, RD = 1 sec, NS = 64, 1 min. wait between experiments. (i) Unipolar Pulses, 1st experiment, (ii) Unipolar Pulses, 4th experiment, (iii) Bipolar Pulses, 1st experiment, (iv) Bipolar Pulses, 4th experiment

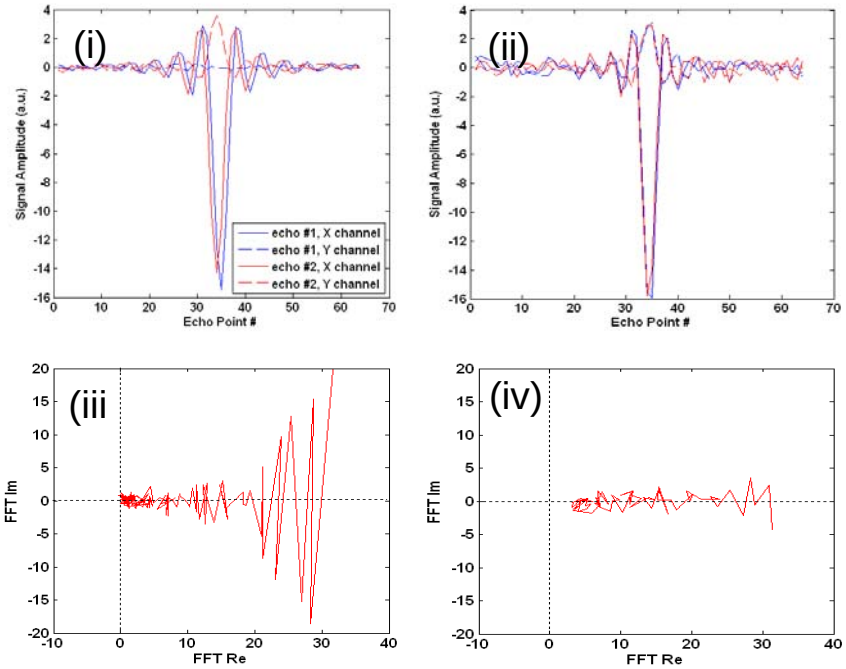

Figure 4: Reduction of phase sensitivity. Squalane, g = 2.5 G cm-1, d = 6 msec. (i) 1st two echoes before inclusion of $\pi/2$ pulse and, (ii)After. (iii) FFT quadrature data of all echoes at h = 1.38 cm echoes before inclusion of $\pi/2$ pulse, and (iv) After.

Table 1: D-T_2 profiling phase cycling list

ϕ_1	ϕ_2	ϕ_3	ϕ_4	ϕ_π	ϕ_{read}
0	0	0	π/2	π/2	π
0	0	π	π/2	π/2	0
0	π	0	π/2	π/2	0
0	π	π	π/2	π/2	π
π/2	π/2	π/2	0	0	3π/2
π/2	π/2	3π/2	0	0	π/2
π/2	3π/2	π/2	0	0	π/2
π/2	3π/2	3π/2	0	0	3π/2
π	0	0	3π/2	3π/2	0
π	0	π	3π/2	3π/2	π
π	π	0	3π/2	3π/2	π
π	π	π	3π/2	3π/2	0
3π/2	π/2	π/2	π	π	π/2
3π/2	π/2	3π/2	π	π	3π/2
3π/2	3π/2	π/2	π	π	3π/2
3π/2	3π/2	3π/2	π	π	π/2

ϕ_1, ϕ_2, ϕ_3, □□□ ϕ_4 represent the phase for the first, second, third, and fourth π/2 pulses, respectively. ϕ_π represents the phase of all of the π pulses and ϕ_{read} is the phase during acquisition.

The phase cycling list implemented with the D-T_2 profiling experiment was selected in order to help minimize the formation of additional echoes typically accompanying the stimulated echo. The sequence suggest by Fauth et al. [16] was implemented and repeated in CYCLOPS fashion resulting in a 16 step list. Table 1 summarizes the phase cycling list utilized for the D-T_2 profiling experiments.

PROCEDURES

Experiments were performed using sandpacks that were 1.7 inches in diameter and 12 inches in length and packed with U.S. Silica 20/40 sand. The sandpack was saturated using the following procedure. First, air was purged from system via CO_2. Next, one pore volume (PV) of water was introduced into the column and allowed to sit overnight. Second, the sandpacked was flushed with 4 PV of water and the permeability measured. Third, Mars Yellow Crude Oil (22 cP) was introduced into the column. Oil saturation of the sand pack was measured to be 0.78 by mass balance. Finally, a waterflood was performed in order to generate a saturation gradient. Both RARE and D-T_2 profiling experiments were performed on the sandpacks after 0.5 PV waterflood. The oil saturation after the partial waterflood was determined to be 0.43 by mass balance. Parameter selection for the imaging portion of the pulse sequence is described in the next sections, and the selected values are summarized in Tables 2 and 3.

Table 2

Diffusion Parameters	
Δ'	60 msec
δ_1	3 msec
δ_3	3 msec
g_D	0.8 to 24.0 G cm^{-1}
τ_L	15 msec

Table 3

Imaging Parameters	
τ	3 msec
g_F	0.8 G cm^{-1}
δ_2	1.3 msec
SI	128
DW	0.016 msec

NMR Parameter Selection

The generation of NMR 1-D profiles is highly dependent upon the selected experimental parameters such as the sample size, gradient strength (g) and duration (δ), the dwell time (DW), and the number of acquisition points (SI). Choosing experimental parameters is not a trivial task since an interdependence of the parameters exists. For example, a long acquisition time will yield a higher resolution image, but will require longer gradient pulses ultimately causing greater diffusion attenuation.

The first step in selecting proper parameters for either of the imaging sequences is to determine the effect of the imaging gradient pulses on the magnetization. Due to the presence of multiple imaging pulses, attenuation due to diffusion can become significant. Therefore, it is necessary to develop a suitable model describing the attenuation in terms of the relevant parameters of the pulse sequences. By implementing the concept of an effective gradient [8] [13], the attenuation equations for both RARE (Equation (2)) and D-T_2 Profiling (Equation (3)) can be determined.

$$M = M_0 \exp\left[-D\gamma^2 g_i^2 \delta_1^2 \left(2(n-1)\tau + \Delta_1 - \frac{2(n-1)\delta_1}{3} \right) \right] \exp\left(\frac{-2n\tau}{T_2} \right) \tag{2}$$

$$M = \frac{M_0}{2} \exp\left(-D\gamma^2 \left[4g_D^2 \delta_1^2 \left(\Delta' - d_g - \frac{2\delta_D}{3} \right) + g_i^2 \delta_2^2 \left(2(n-1)\tau + \Delta_1 - \frac{2(n-1)\delta_2}{3} \right) \right] \right) \exp\left(\frac{-(\Delta' + 2\tau_L)}{T_1} \right) \exp\left(\frac{-2n\tau_S}{T_2} \right) \tag{3}$$

Next, the viable range of parameter space must be determined. These parameters include g, δ, SI and DW. One way to reduce diffusion attenuation is to use weaker gradient pulses. Therefore, it is necessary to properly characterize the behavior of the gradient over a range of values. For instance, at very low gradients, the expected strength of our MARAN's gradient deviates from what is observed. This deviation marks the lower range of reliable gradient strengths, g_{min}. On the other hand, the maximum gradient strength, g_{max}, depends on the probe's bandwidth as well as the height of the sample. Profile rounding can occur when the range of encoded frequencies, Δf, takes up a large portion of the probe's bandwidth. Selection of g_{max} should limit the range of encoded frequencies so that rounding does not occur. In order to determine of Δf_{round}, a single profile of bulk fluid located within the homogeneous region of the probe was generated at 2.0 G cm^{-1}, a value expected to produce a rounded profile. Δf_{round} was taken to be the frequency range corresponding the flat region of the profile.

$$g_{max} = \frac{2\pi \Delta f_{round}}{\gamma \, h_s} \tag{4}$$

The dwell time (DW), or the spacing between the acquired data points, governs the length of investigation by the imaging experiment. Therefore, DW should be selected to acquire data over the length of the sample, h_s, plus a small distance beyond, h_ε. If the dwell time is too short, the distance that the measurement can identify is much longer than the length of the sample. The largest, useable dwell time, DW_{max}, can be determined from the size of the sample and the strength of the imaging gradient pulses applied (equation (5)). This equation is based on the Nyquist sampling theorem [5].

A typical value for h_ε was taken to be 1 cm for a sample. However, when a sample was longer than the length of the probe, the detection length of the probe was used instead of the sum of h_s and h_ε. If this criterion is not meet, aliasing can occur.

$$DW_{\max} = \frac{1}{2f_{\max}} = \frac{2\pi}{\gamma g\left(h_s + h_\varepsilon\right)} \tag{5}$$

The number of acquisition point (*SI*) is also a vital parameter when performing a profiling measurement. While *DW* determined the range of frequencies resolved, *SI* governs the number of points spanning that range. Therefore, the product of *SI* and DW directly impact image resolution.

$$resolution\left[\frac{\text{points}}{\text{cm}}\right] = \frac{\gamma g DW\left(SI-1\right)}{2\pi} \tag{6}$$

However, acquisition must occur under a gradient and is therefore limited by the readout gradient duration (δ_2). Therefore, the duration of the gradient pulse must be greater than or equalled to the product of (*SI*-1) and *DW*. Increasing the gradient duration to accommodate more points will increase resolution at the cost of greater attenuation due to diffusion. Since it is desired to have the highest resolution for a given *DW*, data will be collected for as long as possible. Furthermore, it is desirable to keep *SI* as a power of 2 (i.e., 2^n where n is an integer) because the FFT algorithm is fastest for powers of 2. Therefore, *SI* can be represented

$$SI = 2^{\left[INT\left[\frac{\ln\left(\frac{2\delta_1}{DW}\right)+1}{\ln(2)}\right]\right]} \tag{7}$$

Now that the important parameters have been reviewed, appropriate selection criteria can be introduced. Ultimately, it is desired to produce high-resolution profiles with as little attenuation due to diffusion in the echo train as possible. Equation (2) represents how the acquired signal is impacted by the experimental parameters for the RARE experiment. It can be rewritten in terms of an apparent T_2 relaxation time denoted as $T_2^{\#}$.

$$\frac{T_2^{\#}}{T_2} = \left[1 + DT_2\gamma^2 g^2 \delta_1^2\left(1 - \frac{\delta_1}{3\tau}\right)\right]^{-1}, \qquad n \to \infty \tag{8}$$

For a given g, the maximum resolution occurs when data is acquired during the entire readout gradient or when $2\delta_1 = (SI\text{-}1)DW$. Substituting this relationship into equation (6) demonstrates that resolution is also a function of g and δ_1.

$$resolution\left[\frac{\text{points}}{\text{cm}}\right] = \frac{\gamma g \delta_1}{\pi} \tag{9}$$

Figure 5 shows the resolution as function of g and δ_1 (Equation (8)). Also plotted on the graph are lines of constant ($T_2^{\#}/T_2$). In order to assure that there is not interference between the gradient pulse and subsequent RF pulse, the two are separated by a time d_g. For these calculations, d_g was chosen to be 1millisecond.

$$\tau = \delta_1 + d_g \tag{10}$$

Figure 5 demonstrates that for a given $T_2^{\#}/T_2$, the corresponding image resolution changes only slightly. Therefore, by selecting an acceptable amount of attenuation due to diffusion, the image resolution is set, and a trade off between resolution and $T_2^{\#}/T_2$ ensues. For example, if it is desired to have $T_2^{\#}/T_2 = 0.95$ for a 4 cm water sample, then the resulting image will have a resolution of about 9 points cm^{-1}.

In order to generate a higher resolution image, the RARE signal will undergo more attenuation due to diffusion. By selecting the $T_2^{\#}/T_2$, possible g and δ_1 pairs can be determined. These pairs correspond to the lines of constant $T_2^{\#}/T_2$ in Figure 5. However, not all of the gradient strengths (g) can be used to produce meaningful profiles; a minimum and maximum gradient strength exist for each measurement.

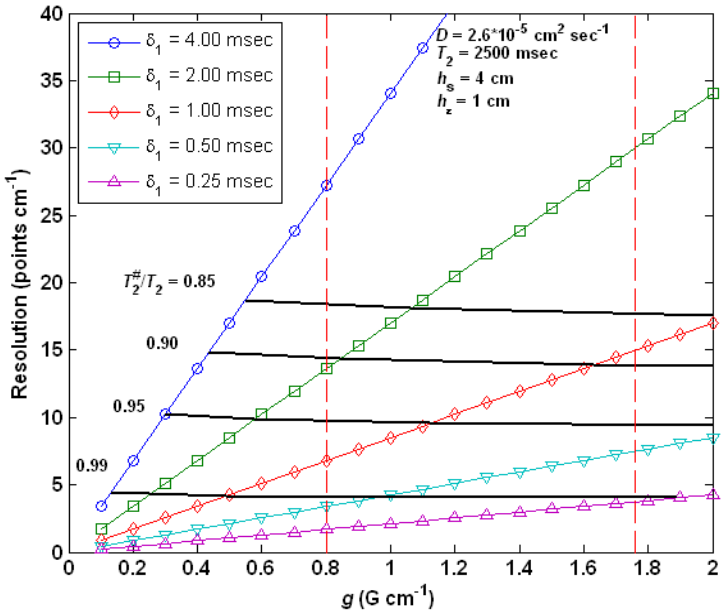

Figure 5: Measurement Resolution with g_{min} and g_{max} denoted by the red, vertical dashed lines

Adding g_{min} and g_{max} to the resolution plot limits the range of possible g and δ_1 (Figure 5). However, a broad range of g and δ_1 pairs still exist for a given $T_2^{\#}/T_2$. The minimum T_2 value to be resolved for the measurement can be used in selecting only a single pair. Since the gradient pulses are between the π-pulses, the echo spacing is limited by the gradient duration. However, the echoes must be spaced close enough in order to resolve the fast relaxing components.

$$2\delta_1 \quad < \quad 2\tau \quad << \quad \min(T_2) \tag{11}$$

If a minimum ratio between echo spacing and min(T_2) is established, a relationship between δ_1 and min(T_2) can be constructed using Equations (10) and (11). Equation (12) represents an arbitrary ratio between δ_1 and min(T_2).

$$\frac{2\tau_{max}}{\min(T_2)} \leq \frac{1}{10} \tag{12}$$

Combining equations (10) into (12) yields equation (13) which is used as the relationship between the minimum T_2 and the gradient duration. Using the largest δ_1 will allow for the longest echo train, and subsequently the broadest resolution of relaxation times. Therefore,

$$\delta_1 = \frac{1}{20}\min(T_2) - d_g \tag{13}$$

With a $T_2^{\#}/T_2$ selected, use of equation (13) should yield a suitable g and δ_1 pair. If, however, this pair lies outside the bounds set by the g_{max} and g_{min} lines, then the selected g and δ_1 pair will correspond to the intersection of the $T_2^{\#}/T_2$ curve and the nearest vertical bound (either g_{max} or g_{min}). Similarly if equation (13) produces a negative value, then the g and δ_1 pair will correspond to the intersection of the $T_2^{\#}/T_2$ curve and

the g_{min} line. In this situation, the fastest relaxing components may not be well resolved. Choosing a value of $T_2^{\#}/T_2$ closer to unity should produce a better measurement of the fastest relaxation times (image resolution should be reduced).

NMR Data Processing

Data collected for both the RARE and D-T_2 profiling experiments are processed in very similar fashions and rely heavily on the application of a fast Fourier transform (FFT). For data collected from a RARE experiment, the first step is to apply an FFT to the two channel data of each echo individually. The frequency scale can then be converted to a length by applying Equation (1). The application of the FFT yields both a real and imaginary signal. The imaginary portion of the profile can be removed by rotating the data. Axis rotation is performed using the transformed data of all the echoes at a single height or frequency. After rotation, the real portion of the data represents the profile while the imaginary portion is a measure of the noise. Now the data is ready to be inverted. However, since the profiles collected via the RARE sequence for bulk fluids have consistently demonstrated a noisy plateau, implementation of a filter is used in order to reduce the noise. The filter used in this study is simply a 3-point weighted average given by Equation (14).

$$\overline{S}(x_i) = w_1 S(x_{i-1}) + w_2 S(x_i) + w_3 S(x_{i+1}) \tag{14}$$

Where $S(x_i)$ is the signal amplitude at the height x_i, $\overline{S}(x_i)$ is the weighted signal average and w_i are the weights used to perform the average. Note that $w_1 + w_2 + w_3 = 1$. For our experiments $w_2 = 0.5$ and $w_1 = w_3 = 0.25$. After averaging, inversion of the data is performed. The profile data at each height is inverted in order to determine a T_2 distribution at that position. For these experiments, the full form of the attenuation equation, Equation (2), was not used. Instead, the diffusion kernel is neglected and an effective relaxation, $T_2^{\#}$, is determined. Proper parameter selection is necessary in order to reduce the effect of attenuation due to diffusion. A common regularization parameter, α, is used throughout the system during inversion. Once the inversion has been performed at each position, the results can be combined into a T_2 map for the measured sample.

Data for the D-T_2 experiments is processed in a very similar manner. The main differences are the need to analyze multiple experiments to determine the effect of diffusion and the application of a 2-D inversion. Once the data from the battery of diffusion editing experiments has been readied for inversion, the profile data at a specific height for all of the experiments performed at varying gradient strengths is inverted using a 2-D inversion. The attenuation equation for the D-T_2 profiling experiment, Equation (3), can still be broken into to two kernels for a 2D inversion [17]. However, the attenuation due to the imaging pulses is neglected during the inversion.

RESULTS

Both T_2 and DT_2 profiles were performed on the sandpack before (Figure 6) and after a 0.5 PV waterflood (Figure 7). Use of the RARE sequence demonstrates that the crude oil and water have overlapping T_2 distributions. However, the two fluids can be identified using D-T_2 profiling. Note that the profiles generated for the sandpack after oilflood were only over a 4 cm.

Saturations can then be determined from each height of D-T_2 profile by comparing the oil signal to the water signal (Equation 15). The calculated saturation profiles for the

sandpack after oilflood and waterflood are presented in Figure 8. As expected the saturation profile is fairly uniform for the sandpack after oilflood. The oil saturation profile average was determined to be 0.76, which is in good agreement with the value obtained by mass balance ($S_{o.mass}$ = 0.78). The profile after the waterflood is not uniform due to unfavourable mobility ratio during the waterflood. Oil saturation at the entrance of the sandpack is near 0.06 and rises to a near constant value of 0.45 near the middle of the sandpack. However, the oil saturation profile average ($S_{o.prof,avg}$ = 0.34) shows a greater disparity from the value determined by mass balance ($S_{o.mass}$ = 0.43) than the oilflood saturation profile.

$$S_o(x) = \frac{\sum_i f_{i,oil}(x, D, T_2) \Big/ HI_{oil}}{\sum_i f_{i,water}(x, D, T_2) + \sum_i f_{i,oil}(x, D, T_2) \Big/ HI_{oil}} \tag{15}$$

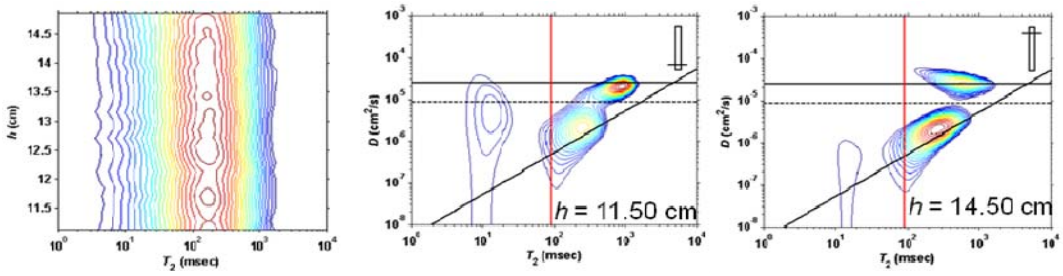

Figure 6: Profiles of sandpack after oilflood. (Left) T_2 profile acquired using the RARE squence, (Center) D-T_2 Profile performed at h = 11.50 cm, and (Right) D-T_2 Profile performed at h = 14.50 cm. The horizontal line indicates the diffusivity of water at 30^{oC}. The line with positive slope represents the D-T_2 correlation for dead oils. The horizontal, dashed line is the division between water and oil used in the saturation calculations. The vertical red line indicates the time at which the first echo was collected

CONCLUSION

Two techniques have been introduced which allow for the generation of 1-D profiles using a low-field Maran spectrometer. The first technique, RARE, allows for the determination of T_2 as function of sample height. The second, D-T_2 profiling, allows for the simultaneous determination of the self-diffusion coefficient, D, and T_2 along the length of a sample. Application of the D-T_2 profiling relied on the use of bipolar gradients in order to generate a good quality and stable echo during the diffusion section of the sequence. Furthermore, it was necessary to insert a $(\pi/2)_y$ pulse into the sequence at the time when the first echo occurs in order to reduce phase instabilities.

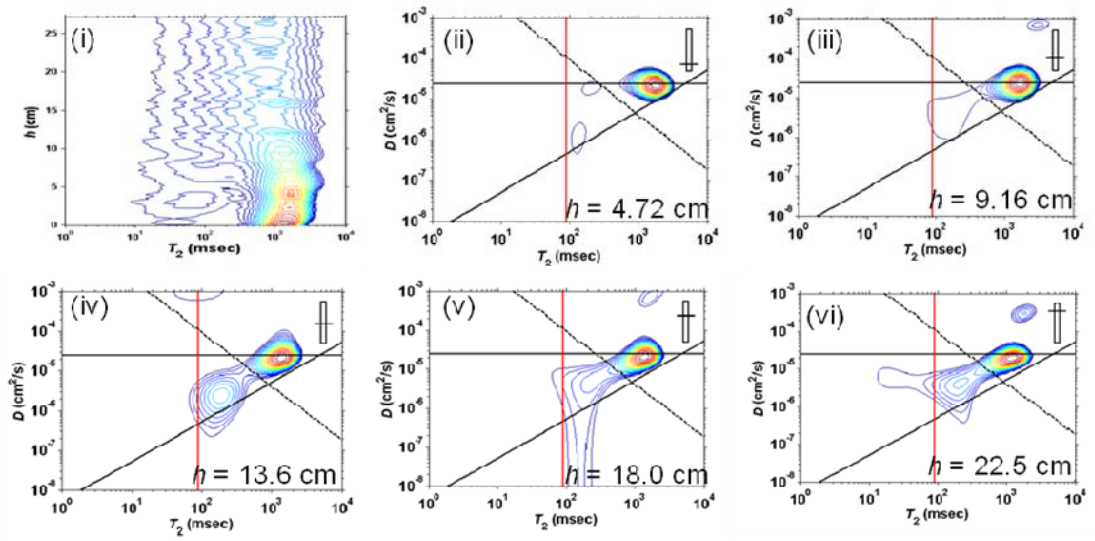

Figure 7: Profiles of sandpack after a 0.5 PV waterflod. (i) RARE profile, (ii) D-T_2 Profile performed at h = 4.72 cm, (iii) h = 9.16 cm, (iv) h = 13.6 cm, (v) h = 18.0 cm, and (vi) h = 22.5 cm.

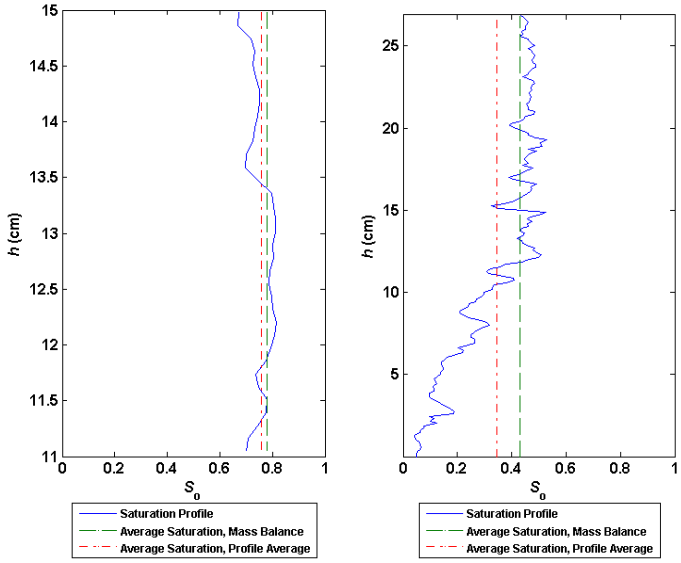

Figure 8: Saturation profiles for (Left) a 4 cm segment of the sandpack after oilflood, and (Right) the entire sandpack after 0.5 PV waterflood.

However, the large echo spacing in the RARE experiments and the diffusion time in the D-T_2 experiments imposes a limitation on measurement of fast relaxing components within a sample. For sandstones, the standard T_2 range for clay bound water, irreducible capillary bound water, and free fluid are less than 3 msec, between 3 msec to 33 msec, and greater than 33 msec, respectively [18]. With an echo spacing on the order of milliseconds, the RARE sequence would not be able to accurately measure a sandstone's clay bound water. Furthermore, the D-T_2 experiments would be insensitive to both the clay bound and irreducible capillary bound water.

REFERENCES

1. Chen, Q. & Balcom, B.J. "*Measurement of rock-core capillary pressure curves using single speed centrifuge and one-dimensional magnetic resonance imaging*," Journal of Chemical Physics, (2005), 122.
2. Green, D.P., Dick, J.R., McAloon, M., de J. Cano-Barrita, P.F., Burger, J., & Balcom, B., "*Oil/water imbibition and drainage capillary pressure determined by MRI on a wide sampling of rocks*," Presented at the International Symposium of the Society of Core Analysts, Abu Dhabi, UAE, (2008).
3. Riskedal, H., Tipura, L., Howard, J., & Graue, A., "*NMR monitoring of spontaneous brine imbibition in carbonates*," Presented at the International Symposium of the Society of Core Analysts, Abu Dhabi, UAE. (2008, October).
4. Johannesen, E., Howard, J., & Graue, A. "*Evaluation of wettability distributions in experimentally aged core*," Presented at the International Symposium of the Society of Core Analysts, Abu Dhabi, UAE, (2008, October).
5. Bernstein, M.A., King, K.F., & Zhou, X.J., *Handbook of MRI pulse sequences*, Elsevier Academic Press, Amsterdam, (2004).
6. Liang, Z.P., & Lauterbur, P.C, *Principles of magnetic resonance imaging: A signal processing perspective,* IEEE Press, New York, (2000).
7. Henning, J., Nauerth, A., & Friedburg, H., "*RARE imaging: A fast imaging method for clinical MRI*," Magnetic Resonance in Medicine, (1986),3, 823-833.
8. Callaghan, P.T. *Principles of nuclear magnetic resonance microscopy*, Oxford University Press, Inc., New York, (1991).
9. Le Bihan, D., Poupon, C., Amadon, A., & Lethimonnier, F., "*Artifacts and pitfalls in diffusion MRI*," Journal of Magnetic Resonance Imaging, (2006), 24(3).
10. Freedman, R., Heaton, N., Flaum, M., Hirasaki, G.J., Flaum, C., & Hürlimann, M., "*Wettability, saturation, and viscosity from NMR measurements*," SPE Journal, (2003), 8(4), 317-327
11. Hürlimann, M., Flaum, M., Venkataramanan, L., Flaum, C., Freedman, R., Hirasaki, G.J., "*Diffusion-relaxtion distribution functions of sedimentary rocks in different saturation states*," Magnetic Resonance Imaging, (2003), 21, 305-310.
12. Flaum, M., Chen, J., & Hirasaki, G.J.. "*NMR diffusion editing for D-T_2 maps: Application to recognition of wettability change*," Presented at the SPWLA 45th Annual Logging Symposium, Noordwijk, Netherlands. (2004, June)
13. Cotts, R., Hoch, M., Sun, T., & Markert, J., "*Pulsed field gradient stimulated echo method for improved NMR diffusion measurement in heterogeneous systems*," Journal of Magnetic Resonance, (1989), 83(2), 252-266.
14. Norris, D., Börnert, P., Reese, T., & Leibfritz, D., "*On the application of ultra-fast RARE experiments*," Magnetic Resonance in Medicine, (1992), 27, 142-164.
15. Alsop, D,. "*Phase insensitive preparation of single-shot RARE: Application to diffusion imaging in humans*," Magnetic Resonance in Medicine, (1997), 38, 527-533.
16. Fauth, J.-M., Schweiger, A., Braunschweiler, L., Forrer, J., Ernst, R.R., "*Elimination of unwanted echoes and reduction of dead time in three pulse electron spin-echo spectroscopy*," Journal of Magnetic Resonance, (1986), 66, 74-85
17. Hürlimann, M., & Venkataramanan, L., "*Quantitative measurement of two-dimensional distribution functions of diffusion and relaxation in grossly inhomogeneous fields*," Journal of Magnetic Resonance, (2002), 157(1), 31-42.
18. Dunn, K.-J., Bergman, D.J., Latorraca, G.A., *Nuclear magnetic resonance: Petrophysical and logging applications*, Pergamon, Amsterdam (2002).